DOI:
10.1039/C7CP01397C

Document Version
Peer reviewed version

Journal Name

ARTICLE TYPE

Cite this: DOI: 10.1039/xxxxxxxxxx

Chemical ordering and mismatch effect on structural transitions in phase segregating nanoalloys

Kevin Rossi, Francesca Baletto

Received Date
Accepted Date

DOI: 10.1039/xxxxxxxxxx

www.rsc.org/journalname

We elucidate the effect of lattice mismatch and chemical ordering on structural transitions in bimetallic nanoalloys of 147 atoms. We show that collective screw dislocation motions happen in small mismatch core-shell systems while strongly mismatched ones favour incomplete outer shell rearrangements. Cooperative transitions can also result hindered when the chemical ordering breaks the geometrical symmetry. The escaping from an unfavourable morphological basin occurs first via a re-arrangements of the geometry and then change towards a better chemical pattern. We observe that the chemical re-ordering mechanisms are independent of system composition and stochiometry but hinge on the initial and final chemical arrangements.

1 Introduction

Nanocluster's architecture and chemophysical properties are intimately related: optical,[1,2] magnetic,[3,4] and catalytic[5,6] features can by tuned by controlling its size, chemical composition and shape, which, in turn are ruled by the delicate interplay of kinetic, entropic and energetic contribution.[7]

Exquisite control over the size and ordering of the nanoalloy is almost at reach,[8–11] however experimental samples are generally polydisperse.[7,12] Both kinetic and entropic effects[13,14] contribute to diversify the architectures resulting from gas-condensation, solidification, synthesis or other methodologies. Structural rearrangement and chemical reordering can take place due to ageing, when nanoalloy is excited under an electron beam, or through thermal annealing. Therefore, it is desirable to predict in which conditions shape fluctuations take place.[11,15–17]

Morphology interconversion processes have been studied for monometallic, core-shell and vertex-decorated systems by means of transition state search algorithms, molecular dynamics or enhanced sampling techniques.[18–28] It has been shown that solid-solid transitions of cuboctahedral (Co) or decahedral (Dh) morphologies into icosahedral (Ih) one happens in nanoclusters, with sizes as small as 147 atoms, via cooperative screw-dislocation motions also known as diamond-square-diamond (DSD) rearrangements.[29,30].

A few studies investigated the dynamics of chemical reordering, targeting only subnanometer nanoalloys.[31,32] They identified two possible rearrangement mechanisms: surface peeling and atomic inter-diffusion.[33] The former consists of elementary steps of surface diffusion and displacements and leads to segregated-segregated transformations. The latter comprises vacancy formation and atomic intracluster diffusion and takes place in segregated-mixed transition.

In this work, we systematically analyse finite temperature solid-solid transitions and chemical reordering in AgPt and AgCu nanoclusters with a diameter of ∼1.8 nm presenting a variety of architectures. In particular we characterize morphological rearrangement and chemical reordering mechanisms in core-shell and Janus nanoclusters, through a systematic analysis of several different order parameters which encode detailed information about the structure, chemical species arrangement and transition kinetics. We investigate solid-solid transition mechanisms in AgPt and AgCu clusters because of their fascinating catalytic and optical properties and the large number of previous optimization and kinetic studies on them.[34–37] Our numerical approach offers a fertile perspective to address how mismatch (3% for AgPt and 12% AgCu), and chemical ordering influence rearrangements in the cluster.

We find that structural transitions among the Ih, Dh, and Co geometries happen in small mismatched core-shell nanoalloys via the same cooperative screw dislocation motions as in their monometallic counterparts. On the other hand, these mechanisms are hindered in strongly mismatched systems. They might also be altered in systems where the chemical ordering violates the geometrical symmetry: starting from an unfavourable shape with a Janus chemical ordering, for example, the rearrangements are constrained by the Janus cut. We further note that morphological inter-conversions always precede chemical reordering in systems presenting both high energy geometries and chemical ordering. Finally, we show that regardless of nanoalloy initial

[a] King's College, Physics Department, Strand WC2R 2LS, London, United Kingdom, E-mail: kevin.rossi@kcl.ac.uk

† Electronic Supplementary Information (ESI) available: [details of any supplementary information available should be included here]. See DOI: 10.1039/b000000x/

shape and mismatch surface diffusion happens during segregated-segregated phase transition, while atomic intercluster diffusion in chemical reordering processes which involve mixed phases.

2 Models and Methods

The considered architectures are reported in Figure 1, where the "@" stand for a core@shell ordering and the "||" is used for referring to a Janus pattern. We fix the size at 147 atoms and choose to focus on structural changes and chemical reshuffle of a silver outer shell over a Cu or Pt core, likely to be the favourable chemical ordering[36,37] and a Janus order with a cut along the (100) facet of a Co and perpedicular to the five-fold axis for a Dh. In the case of a Janus architecture, we consider an almost 50% stoichionetry. The rationale behind our system's choice is to assess the mismatch effect in the case of both spherically and non-spherical chemical pattern and to address the competition between structural and chemical rearrangement mechanisms.

To investigate structural transitions in bimetallic nanoalloys we couple molecular dynamics (MD) with a Metadynamics (MetaD) algorithm or an iterative temperature scheme (itMD). Newton's equation of motions are solved using a velocity-Verlet algorithm with a time step of 5 fs while an Andersen thermostat regulates the temperature of the system. Metal-Metal interactions are modelled within the second moment tight binding approximation[38] potential and the employed parametrization follows the literature.[36,37]

ItMD consists of a series of concatenated MD runs where the temperature is slowly increased at a constant rate. Here, we choose by leave the system free to move for at least 1 ns before the temperature is increased of 50 K. We start from tempeartures as low as 100K up to the melting transition. The 1 ns time frame is sufficient long to observe several changes and to characterise the appearance of any martensitic transition[39].

MetaD exploits a history dependent potential, built by summing Gaussians in a collective variables (CVs) space, to enhance the exploration of the conformational space of the system and eventually reconstruct its free energy.[40] As discussed in our recent work,[25] we can use two window functions (WF), set at characteristic distances of the pair distance distribution function (PDDF), to investigate structural transitions in nanoclusters. Those CVs are evaluated as:

$$WF = \sum_{i,j;i\neq j} \frac{1-\left(\frac{r_{ij}-d_0}{r_0}\right)^6}{1-\left(\frac{r_{ij}-d_0}{r_0}\right)^{12}}, \tag{1}$$

with r_{ij} being the distance between the i and j atoms, r_0 the window width, and d_0 the characteristic position. In bimetallic systems, depending on the chemical type of the i and j atom, we consider the corresponding bulk lattice parameter or, for hetero-pairs, their average. The first window function is set to the characteristic hcp peak ($\sqrt{8}/3$) to count the stacking fault number and enhances sliding and rotation of (111) planes; the second one, positioned at around the 5^{th} neighbours distance, is correlated to breathing and sliding mechanisms. For this choice of CVs, the MetaD potential evolves every 10 ps by the deposition of a Gaussian tall 0.15 eV with a system dependent width, in the 20-30 range.

The two window functions do not distinguish precisely among two clusters presenting the same shape but a different chemical ordering, as an example, $Ag_{92}@Pt_{55}$ Ih is projected at (956,1155) while a $Ag_{82}||Pt_{65}$ Ih is found at (1025,1204), with only a few Gaussian dividing them. More importantly, these collective variables boost poorly any movements via single atomic diffusion, which is the elementary step by which chemical reordering results.[33] As the coordination number is a robust CV to drive the latter mechanism[41,42], we propose the hetero and homo coordinations numbers as efficient CVs to simulate chemical reordering via single atom intracluster or surface diffusion. Let p_0 be the nearest neighbour bulk reference distance, q_0 as the distance related to the width of the descending branch of a sigmoid function f, and n and m as the powers used to tune smoothness and asymptotic behaviour of the analytic function f, the hetero coordination number, HeCN, results:

$$HeCN = \sum_{i,j} \sum_{i\neq j} f(r_{ij}),$$

$$f(r_{ij}) = \begin{cases} 1 & \text{if } r_{ij} \leq p_0, \\ \dfrac{1-\left(\frac{r_{ij}-p_0}{q_0}\right)^n}{1-\left(\frac{r_{ij}-p_0}{q_0}\right)^m} & \text{if } r_{ij} > p_0, \end{cases} \tag{2}$$

The same analytical formulation, with an appropriate choice for p_0, holds for the homo-atomic coordination, HoCN. The Janus and core-shell structures are well separated along the HeCN collective variable, the latter being at 476, for $Ag_{92}@Pt_{55}$, and the former at 253, in the case of $Ag_{86}||Pt_{61}$. When HeCN (Ag-M, M=Pt, Cu) is employed as unique CV, the Gaussians are deposited every 10 ps, are 0.1 eV tall and 2 wide. Although using the HeCN as sole collective variables enables to sample efficiently minima with various chemical ordering and energy differences of several eV, it does not encode enough information to discriminate among nanoparticle shapes. This implies that clusters presenting differ-

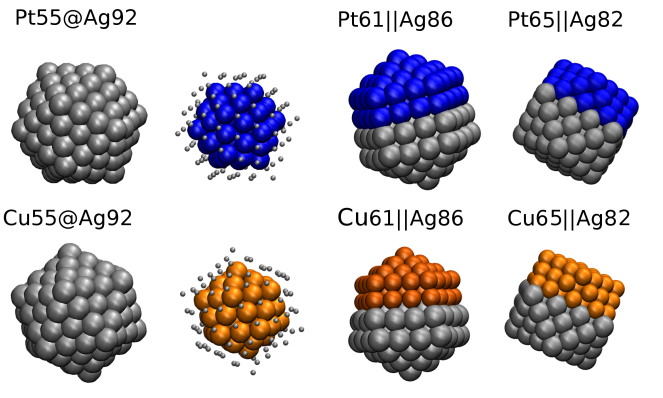

Fig. 1 AgPt (top) and AgCu (bottom) nanoalloys: an Ih with a core@shell ordering with a Ag outershell and a view of the 55-atoms core; Janus-Dh with a cut perpendicular to the 5-fold axis (middle), and a Janus-Co with a cut along a (100) plane (right). Ag, Pt, and Cu atoms are coloured respectively in silver, blue, and orange.

ent motifs but similar chemical ordering are projected onto the same basin, hampering the possibility to reconstruct correctly the free energy profile.

2.1 Architecture and Kinetics Characterization

Nanoalloy morphology is monitored by means of the Common Neighbour Analysis (CNA)[43] which characterizes the local connectivity around each pair of nearest neighbours in the system. It associates to them a signature (r,s,t) dependent on the connectivity of their neighbourhood: r is the number of their common neighbours, s the number of bonds between the r atoms, and t the longest chain among them. The (4,2,2) CNA signature is assigned to pairs along grain boundaries and is used here to distinguish among different morphologies.

The degree of mixing between the chemical species is probed by the segregation parameter μ.[44] It is defined as:

$$\mu = \frac{HoCN - HeCN}{HoCN + HeCN} \quad . \tag{3}$$

μ takes a value of 1 for fully segregated systems and -1 for fully ordered mixed systems. Phase segregated or mixed arrangements are respectively identified by a positive or negative mixing parameter value.

The spatial distribution of the two chemical species is instead encoded in the chemical radius of gyration, G^{α}:

$$G^{\alpha} = \sqrt{\frac{1}{N^{\alpha}} \sum_{i \in \alpha} (rcom_i)^2} \, , \tag{4}$$

where α distinguishes the chemical species of interest, N^{α} is the total number of α atoms, and $rcom_i$ is the distance of the atom i, belonging to chemical species α, from the center of mass of the whole cluster.

To provide an estimate of the mobility of a chemical species during a reordering processes we contrast the nearest neighbour adjacency matrix of the system, $M_{ij}(t)$ at two different time steps t and $t+\Delta t$. $M_{ij}(t)$ is a N by N matrix, with N being the total number of atoms in the system, with entries equal to 1 or 0 depending on whether the distance between atom i and atom j falls below or above the nearest neighbour distance. The latter is set at the intermediate distance between the first two peaks of the pair distance distribution function of the α chemical species. The overall mobility of a chemical species during a rearrangement can be estimated by counting the total number of homo-rearrangements:

$$R^{\alpha}(t, t+\Delta t) = \sum_{i \in \alpha, j \neq i} R_i^{\alpha}(t, t+\Delta t) \, , \tag{5}$$

R_i^{α} being the atomic homo-rearrangements index:

$$R_i^{\alpha}(t, t+\Delta t) = \sum_{i,j \in \alpha, j \neq i} |M_{ij}^{\alpha,\alpha}(t+\Delta t) - M_{ij}^{\alpha,\alpha}(t)| \, . \tag{6}$$

No structural or chemical ordering changes around the atom i correspond to a $R_i^{\alpha}(t, t+\Delta t) = 0$, while a full rearrangement in the neighbourhood of an fcc bulk atom within a time step Δt, instead lead to $R_i^{\alpha}(t, t+\Delta t) = 24$, twice the bulk nearest neighbours.

To quickly monitor the starting of a chemical reshuffling, a useful quantity is the ratio of atoms of species α who change at least one of their first neighbours, H^{α},

$$H^{\alpha} = \sum_{i \in \alpha}^{N^{\alpha}} \frac{\Theta(R_i^{\alpha}(t, t+\Delta t))}{N^{\alpha}} \begin{cases} \Theta(0) = 0 \\ \Theta(R_i^{\alpha}) = 1 \; \forall \; R_i^{\alpha} > 0 \, . \end{cases} \tag{7}$$

H^{α} ranges between [0,1], $H^{\alpha} = 0$ when no homo-atomic pair has changed, $H^{\alpha} = 1$ when every α atom has at least one change in its neighbourhood, within a time step Δt. A final comment on the time-scale over which structural transitions should be monitored. As a typical period for adatom diffusion on flat surface is expected to be close to 10 ps, we choose Δt equal to 10 ps, as self-adatom diffusion is the fastest rearrangement process we would like to monitor.

3 Results and Discussion

3.1 Mismatch effect on morphological rearrangements

The mismatch between chemical species in the nanoalloy affects the rearrangement kinetics of solid-solid transtions among closed-shell polyhedra, as in the $Pt_{55}@Ag_{92}$ and $Cu_{55}@Ag_{92}$ cases, as depicted in Figure 2. Let us first discuss the reconstruction in a small mismatched alloy as the $Pt_{55}@Ag_{92}$. The evolution of the (4,2,2) CNA signature for the whole cluster and the 55-atoms core. Ih $\leftrightarrow$ Co and Ih $\leftrightarrow$ Dh transitions via DSD mechanism happen simultaneously in the inner Pt-core and in the Ag outer shell, and they proceed exactly as in the case of monometallic systems[25]. The (100) facets of the Dh or Co first deform into a (111) diamond, which after a collective rotation of the atoms in the cluster become two distinct and adjoint (111) facets of an Ih. The inverse process, although more energetically expensive is also feasible. The free energy barriers for the Co $\rightarrow$ Ih (Co $\leftarrow$ Ih) transitions is of 0.25 eV (3.6 eV). A partial overlap between the Ih and Dh conformational basins appears due to the sampling of intermediate defected structures, we heuristically determine an upper bound on the barriers dividing the two geometries, 1.5 eV (4.3 eV) for the Dh$\rightarrow$Ih (Ih$\leftarrow$Dh) transition, by summing up the amount of MetaD potential needed to escape the initial Dh (Ih) basin.

A different mechanism is observed in the case of large mismatched alloy as $Cu_{55}@Ag_{92}$. In this case, the geometric constrains imposed by the mismatch undermine the completion of the DSD rearrangement in the cluster outer shell. As shown in Figure 2, the (4,2,2) CNA signature of the whole cluster does not correspond to the ones for perfect Dh and Co clusters of 147 atoms, yet the Cu_{55} core assumes a Dh and Co geometry. While the Cu core undergoes a clear Ih $\rightarrow$ Dh or Ih $\rightarrow$ Co transition following a DSD mechanism, this movement is not possible for the Ag external shell which displays twin capped motifs. This novel family of rearrangement mechanisms resembles the shell-wise Mackay transformations first reported in Fe_{561} large-scale DFT optimization.[45] The so sampled Dh@Ih and Co@Ih structures result a few eV more favourable than the perfect Dh and Co structures. We notice that the Cu inner core still perform a DSD movement with a barrier as low as 0.1 eV, similarly to the one find in the case of pure Cu_{55}.[46] The fact that the Cu_{55}-core has a similar barrier in the gas phase and covered by an Ag outer shell suggests a weak interaction between the two parts of the clusters.

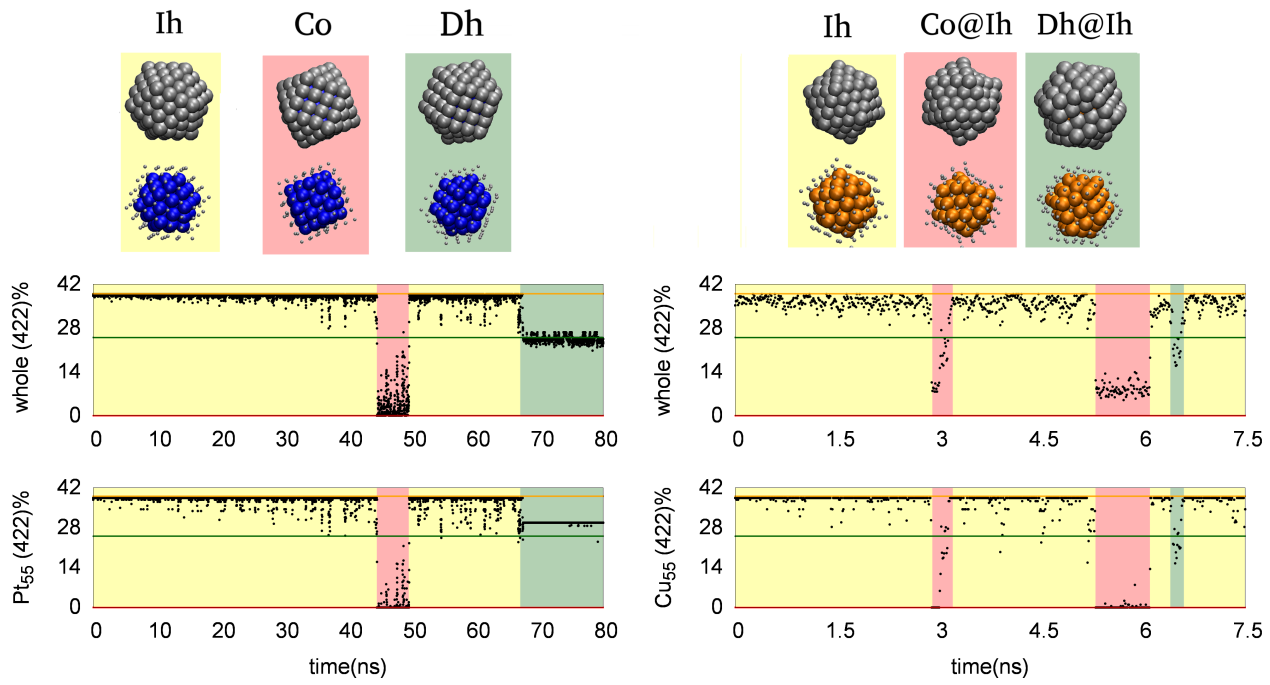

Fig. 2 (422) CNA signature percentage for whole cluster (top) and 55 atoms core (bottom) for $Pt_{55}@Ag_{92}$ (right) and $Cu_{55}@Ag_{92}$ (left) during the course of MetaD runs at 300K. Reference values for ideal Ih, Dh, and Co geometries are shown via a straight gold, green and red line. When Ih, Dh and Co geometries are sampled, the plot is highlighted in yellow, dark-green or pink. A representative snapshot for each of the above mentioned geometries is reported. Atoms colour coding follows from Figure 1.

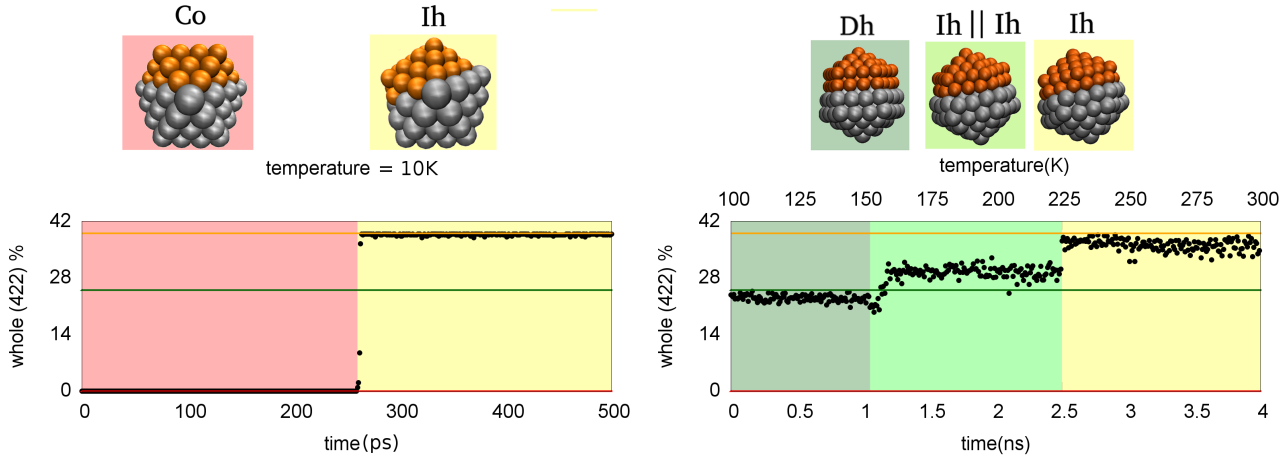

Fig. 3 (422) CNA signature percentage for a Co (left) or Dh (right) → Ih transition in Janus $Ag_{82}||Cu_{65}$ and $Ag_{86}||Cu_{61}$ for during itMD runs. Reference values and window colouring scheme is the same as in Figure 2. The mis-stacked half-Ih||half-Ih sampled during the structural rearrangement of $Ag_{86}||Cu_{61}$ is also reported and highlighted in light-green.Atoms colour coding follows from Figure 1.

3.2 Chemical ordering effect on morphological rearrangements

In Figure 3 we report two paradigmatic examples of the transition from Janus Co and Dh geometries towards a Janus Ih, in the case of AgCu. We stress from the beginning that the same rearrangement mechanisms are observed also for AgPt clusters, showing a negligible role of the mismatch in this case. Furthermore and quite interestingly, we observe that geometrical reconstructions towards more energetically favourable structures, as the Ih, always precede chemical reordering. In addition, we find that these geometrical transitions are martensitic and happens below room temperature. The DSD in Co→Ih transitions happens by the twisting and the stretching of the square facets, around an axis which goes through the center of the triangular facets. The Janus cut in the Co is always parallel to two square (100) facets and perpendicular to the other two, similarly triangular (111) facets are split among pure Ag and Cu-rich presenting either an Ag edge or vertex. The DSD mechanism leads to the splitting of the two mixed square (100) facets in four mixed triangular (111) facets.

In the case of Dh, we notice a new mechanism. The Janus cut

is along (100) interface, perpendicular to the 5-fold axis. The axis is maintained during the transformation towards a Ih. However, the pathway is not any longer the concerted DSD, but steps throughout the formation of an intermediate mis-stacked half-Ih || half-Ih (Ih||Ih) morphology which then undergoes a species-by-species screw dislocation motion to form a perfect Ih geometry. Indeed, the two halves do a separate DSD motion along the same 5-fold axis but rotating in opposite directions resulting first into a (100) interface between silver and copper regions. A final rotation of one species with respect the other completes the formation of a Janus Ih.

We would like to stress that below room temperature, and in the few ns timescale, no chemical changes take place on both AgCu and AgPt nanoalloys even if starting from a Janus pattern, although it is energetically unfavorable. Apparently the reordering of a Janus- rearrangement takes place closed to the melting transition. We do not exclude that an unfavourable chemical pattern may have a lower melting point and then the nanoparticle can fluctuate between solid/liquid configurations with a better chemical ordering. More calculations are needed to see if there is a coexistence of janus and core-shell ordering around 600-650K which is the temperature window just below the melting of core-shell, Ag@Cu melts at 650K while the pure cases at 750K pure Cu and 660K pure Ag; but a single Cu impurity in Ag 147 showed an increment of the melting point up 20-25K due to a release of the internal strain.[47]

3.3 Chemical reordering mechanisms

To show that the initial and final chemical order sampled determine whether surface adatom diffusion or intershell diffusion takes place, with a little influence of the mismatch and the initial geometry, let us analyse the paradigmatic case of structural and chemical evolution in Dh $Ag_{86}||Cu_{61}$ via an itMD procedure. Figure 4 reports the evolution of the structural order parameter ((4,2,2) CNA signature) and chemical characterization (segregation parameter μ and chemical radius of gyration G^{α}) as well as the evolution of H^{α} and R^{α} descriptors to detail the kinetics of the reorganization. After the first 3 ns we observe the aforementioned structural transition from Dh to Ih through the mis-stacked Ih||Ih configuration where only a Cu-layer rotates, followed by the Ag-region which finalises the rotation towards the Janus-Ih (Figure 3). This motif results to be a long-lived metastable one surviving up to 450 K. At this temperature, the Ag cap starts to disorder and surface defects appear and surface diffusion onto (111) facets processes start. We do indeed expect that for the considered metals, surface diffusion on (111) surfaces is more favourable with respect to the (100) ones.[48] Just below 600 K, the chemical reordering from the defected Janus cluster to a defected core-shell arrangement takes place via several atomic surface diffusion and inter-cluster rearrangements. In the initial steps of the reordering process, the mobility of Ag atoms is larger with respect to Cu, both in terms of number of Ag atoms modifying their connectivity and the number of bonds changed. Afterwards, when a highly defected core-shell structure arrangement is observed, both Ag and Cu networks undergo strong rearrangements.

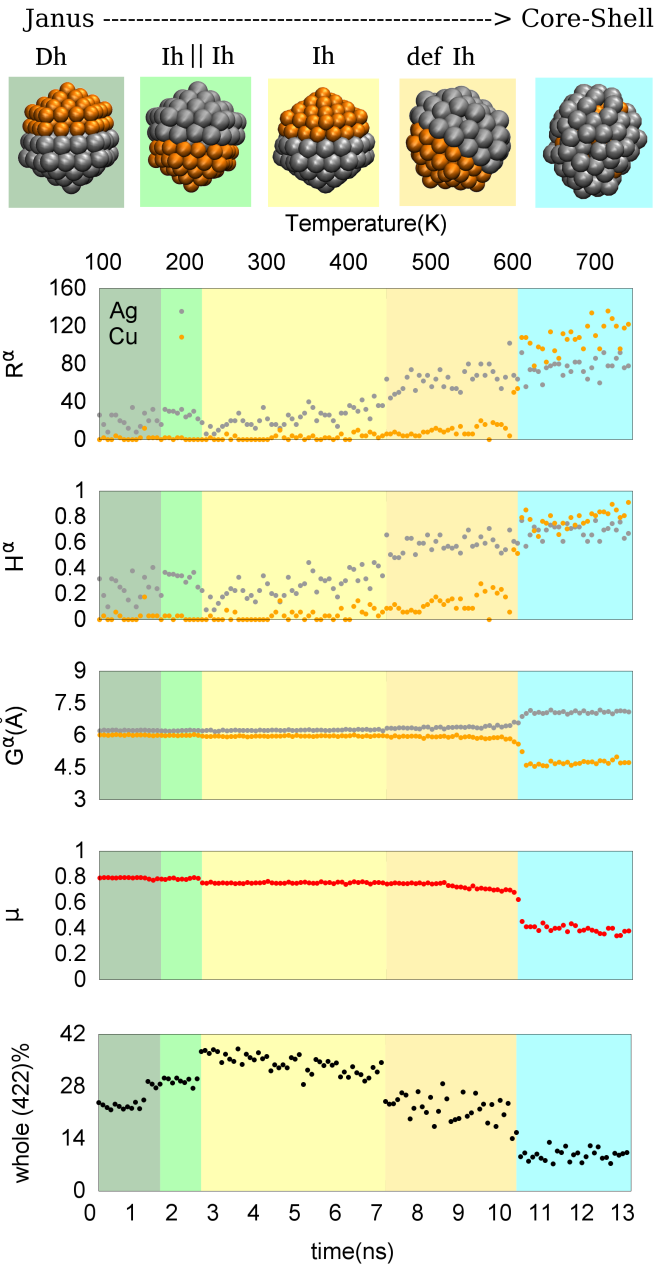

Fig. 4 Janus → core-shell transition in $Ag_{85}Cu_{62}$, obtained during an itMD procedure. Five regimes are found, highlighted by coloured regions, in correspondence of increments and plateaus in the (4,2,2) CNA signature. Snapshots of representative geometries in each region are shown in the top row. From the R^{α} and H^{α} parameters we infer that Ag is initially more mobile while the full chemical reordering is evident only at 600K corresponding to a strong change in the segregation parameter for Ag (in grey) and Cu (in orange).

Thanks to the introduction of the HeCN as unique collective variable, chemical reordering transitions can be sampled by means of Metadynamics. As an example of how we can enhance the sampling of various chemical patterns, we report in Figure 5 the evolution of μ and G^{α} during a 200 ns run for $Pt_{55}Ag_{92}$, where the initial configuration is a perfect Ih core-shell structure. We observe reordering in the inner shells of the cluster, as signalled by the increasing radius of gyration in Pt and the decrease

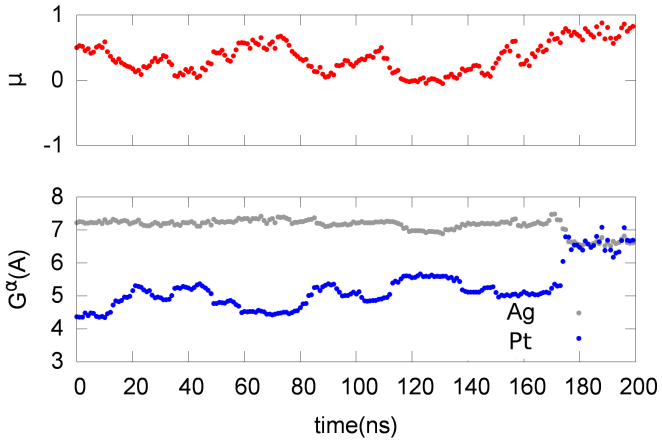

Fig. 5 Evolution of the chemical radius of gyration (G^{α}), for Ag (silver) and Pt (blue) and of the segregation parameter (μ) during a HeCN driven MetaD run at 300K starting from an Ih Ag_{92}@Pt_{55}.

of the segregation parameter, corresponding to an increase in the hetero bonds. During such rearrangements, the outer shell is always Ag-rich, if not made only of Ag atoms, the two inner shells are Pt-rich, occasionally also an Ag@Pt@Ag multi-shell ordering is sampled, as in the 140-160 ns time interval. At 160ns, a similar radius of gyration for Ag and Pt, joint to a increase in the segregation parameter, corresponds to the transition towards a Janus pattern.

Our simulations show further that core-shell $\leftrightarrow$ Janus reordering transition happen via surface adatom diffusion while random mixing $\leftrightarrow$ core-shell ones take place via vacancy formation and intracluster atomic diffusion, in agreement with previous studies.[31] The two mechanisms can happen simultaneously and lead to a variety of reordering pathways which connect, for example, mixed to Janus arrangements or multi-shell to core-shell patterns.

4 Conclusion

We show a rich panorama of rearrangement mechanisms in nanoalloys at 147 atoms by means of enhanced sampling techniques. We address how chemical ordering and mismatch affect structural transition pathways among different morphologies. To sample more efficiently chemical transitions, we have introduced the hetero-atomic coordination number as a sole collective variable of a Metadynamics framework because of its ability to enhance both surface and intra-cluster diffusion happen. We remark that the chemical coordination numbers are order parameters which may be easily transferable to enhance the sampling of a variety of systems where (de)alloying processes or mixing-segregation transitions are of interest. We introduce proper and new descriptors to characterize the mobility of the two chemical species during the structural and chemical reconstruction. The application of those quantities is not limited to this study, they can be applied to characterize kinetics of other systems, as they depend only on the evolution of the system adjacency matrix.

When analyzing the several identified rearrangement pathways we observe that the Diamond-Square-Diamond[29] path connects Ih to Co and Dh morphologies in core-shell nanoalloys when the mismatch is less than 10%. *Viceversa*, an incomplete Diamond-Square-Diamond rearrangement, similar to the shell-wise Mackay[45] mechanism, takes place in system characterised by a larger mismatch. Structural transitions in Janus nanoalloys result shape dependent: while Co rearranges into an Ih via the DSD mechanism, this cooperative screw dislocation motion is hindered in Dh where the formation of (111) interfaces between the two chemical species is the first step of a species-by-species rotation around the 5-fold axis leading to the formation of a Janus Ih, which is rather stable up to 450 K. Opposite to morphological rearrangements, which involves rotations, screw and concerted motion, chemical reordering takes place via surface and/or intra-cluster diffusion regardless of the system's composition. We note that a metastable minimum first underwent a transition towards a favourable geometry and only then chemical reordering starts, thus providing a design criterion to prevent or at least delay the latter.

References

1 M. I. Stockman, *Science*, 2015, **348**, 287–8.
2 G. Barcaro, L. Sementa, A. Fortunelli and M. Stener, *Physical chemistry chemical physics : PCCP*, 2015, **17**, 27952–67.
3 V. M. Medel, J. U. Reveles, S. N. Khanna, V. Chauhan, P. Sen and A. W. Castleman, *Proceedings of the National Academy of Sciences of the United States of America*, 2011, **108**, 10062–6.
4 C. Di Paola, R. D'Agosta and F. Baletto, *Nano Letters*, 2016, **16**, 2885–2889.
5 F. Calle-Vallejo, J. Tymoczko, V. Colic, Q. H. Vu, M. D. Pohl, K. Morgenstern, D. Loffreda, P. Sautet, W. Schuhmann and A. S. Bandarenka, *Science*, 2015, **350**, 185–189.
6 G. G. Asara, L. O. Paz-borbon and F. Baletto, *ACS Catalysis*, 2016, **6**, 4388–4393.
7 F. Baletto and R. Ferrando, *Reviews of Modern Physics*, 2005, **77**, 371–423.
8 S. R. Plant, L. Cao and R. E. Palmer, *Journal of the American Chemical Society*, 2014, **136**, 7559–62.
9 S. Scaramuzza, S. Agnoli and V. Amendola, *Physical Chemistry Chemical Physics*, 2015, **17**, 28076–28087.
10 Z. Swiatkowska-Warkocka, A. Pyatenko, F. Krok, B. R. Jany and M. Marszalek, *Scientific reports*, 2015, **5**, 9849.
11 Z. W. Wang and R. E. Palmer, *Physical Review Letters*, 2012, **108**, 245502.
12 A. S. Barnard, *Nanoscale*, 2014, **6**, 9983–90.
13 F. Baletto, J. P. K. Doye and R. Ferrando, *Physical Review Letters*, 2002, **88**, 075503.
14 F. Baletto, A. Rapallo, G. Rossi and R. Ferrando, *Physical Review B*, 2004, **69**, 235421.
15 K. Koga, T. Ikeshoji and K.-i. Sugawara, *Physical Review Letters*, 2004, **92**, 115507.
16 Shibata T., Bunker B. A., Zhang Z., Meisel D., Vardeman C. F. and Gezelter J. D., *Journal of the American Chemical Society*, 2002, **124**, 11989–11996.
17 C. Wang, S. Peng, R. Chan and S. Sun, *Small*, 2009, **5**, 567–570.

18 J. Uppenbrink and D. J. Wales, *Faraday Transactions*, 1991, **87**, 215.
19 L. D. Marks, *Reports on Progress in Physics*, 1994, **57**, 603–649.
20 D. J. Wales and L. J. Munro, *Journal of Physical Chemistry*, 1996, **100**, 2053–2061.
21 B. Cheng and A. H. W. Ngan, *Journal of Chemical Physics*, 2013, **138**, 164314.
22 Y. K. Lan, C. H. Su, W. H. Sun and A. C. Su, *RSC Advances*, 2014, **4**, 13768.
23 T. Li, S. Lee, S. Han and G. Wang, *Physics Letters A*, 2002, **300**, 86–92.
24 Z. Zhang, W. Hu and S. Xiao, *Physical Review B*, 2006, **73**, 125443.
25 L. Pavan, K. Rossi and F. Baletto, *Journal of Chemical Physics*, 2015, **143**, 184304.
26 F. Chen and R. L. Johnston, *Applied Physics Letters*, 2008, **92**, 023112.
27 A. L. Gould, A. J. Logsdail and C. R. A. Catlow, *Journal of Physical Chemistry C*, 2015, **119**, 23685–23697.
28 A. L. Gould, K. Rossi, C. R. A. Catlow, F. Baletto and A. J. Logsdail, *The Journal of Physical Chemistry Letters*, 2016, **7**, 4414–4419.
29 W. N. Lipscomb, *Science*, 1966, **153**, 373–8.
30 A. L. Mackay, *Acta Crystallographica*, 1962, **15**, 916–918.
31 F. Calvo, A. Fortunelli, F. Negreiros and D. J. Wales, *The Journal of Chemical Physics*, 2013, **139**, 111102.
32 M. Asgari, F. R. Negreiros, L. Sementa, G. Barcaro, H. Behnejad and A. Fortunelli, *The Journal of chemical physics*, 2014, **141**, 041108.
33 T. Niiyama, S. Sawada, K. S. Ikeda and Y. Shimizu, *Chemical Physics Letters*, 2011, **503**, 252–255.
34 W. He, X. Wu, J. Liu, K. Zhang, W. Chu, L. Feng, X. Hu, W. Zhou and S. Xie, *Langmuir*, 2010, **26**, 4443–4448.
35 D. Bochicchio and R. Ferrando, *The European Physical Journal D*, 2012, **66**, 115.
36 R. L. Johnston, L. O. Paz-Borbón, G. Barcaro and A. Fortunelli, *Journal of Chemical Physics*, 2008, **128**, 134517.
37 K. Laasonen, E. Panizon, D. Bochicchio and R. Ferrando, *Journal of Physical Chemistry C*, 2013, **117**, 26405–26413.
38 V. Rosato, M. Guillope and B. Legrand, *Philosophical Magazine A*, 1989, **59**, 321–336.
39 D. J. Wales and P. Salamon, *Proceedings of the National Academy of Sciences*, 2014, **111**, 617–622.
40 A. Laio and F. L. Gervasio, *Reports on Progress in Physics*, 2008, **71**, 126601.
41 G. Santarossa, A. Vargas, M. Iannuzzi and A. Baiker, *Physical Review B - Condensed Matter and Materials Physics*, 2010, **81**, 174205.
42 L. Pavan, C. Di Paola and F. Baletto, *European Physical Journal D*, 2013, **67**, 24.
43 J. D. Honeycutt and H. C. Andersen, *Journal of Physical Chemistry*, 1987, **91**, 4950–4963.
44 F. Calvo and C. Mottet, *Physical Review B*, 2011, **84**, 035409.
45 G. Rollmann, M. E. Gruner, A. Hucht, R. Meyer, P. Entel, M. L. Tiago and J. R. Chelikowsky, *Physical Review Letters*, 2007, **99**, 083402.
46 K.Rossi, Y.Soon, L.Pavan and F.Baletto.
47 C. Mottet, G. Rossi, F. Baletto and R. Ferrando, *Physical Review Letters*, 2005, **95**, 035501.
48 S. Y. Kim, I.-H. Lee and S. Jun, *Physical Review B*, 2007, **76**, 245407.